Human Molecular Genetics, 2006, Vol. 15, No. 19 ***2962–2971***
doi:10.1093/hmg/ddl239
Advance Access published on September 8, 2006

Depletion of type IA regulatory subunit (RIα) of protein kinase A (PKA) in mammalian cells and tissues activates mTOR and causes autophagic deficiency

Manos Mavrakis[1,*], Jennifer Lippincott-Schwartz[1], Constantine A. Stratakis[2] and Ioannis Bossis[2]

[1]Cell Biology and Metabolism Branch, National Institute of Child Health and Human Development, National Institutes of Health, Room 101, Building 18T, 18 Library Drive, Bethesda, MD 20892, USA and [2]Section on Endocrinology and Genetics, Developmental Endocrinology Branch, National Institute of Child Health and Human Development, National Institutes of Health, Building 10, CRC, 10 Center Drive Bethesda, MD 20892, USA

Received July 13, 2006; Revised and Accepted August 24, 2006

The human *PRKAR1A* gene encodes the regulatory subunit 1-alpha (RIα) of the cAMP-dependent protein kinase A (PKA) holoenzyme. Regulation of the catalytic activity of PKA is the only well-studied function of RIα. Inactivating *PRKAR1A* mutations cause primary pigmented nodular adrenocortical disease (PPNAD) or Carney complex (CNC), an inherited syndrome associated with abnormal skin pigmentation and multiple neoplasias, including PPNAD. Histochemistry of tissues from CNC patients is indicative of autophagic deficiency and this led us to investigate the relationship between RIα and mammalian autophagy. We found that fluorescently tagged RIα associates with late endosomes and autophagosomes in cultured cells. The number of autophagosomes in *prkar1a*$^{-/-}$ mouse embryonic fibroblasts (MEFs) was reduced compared with wild-type MEFs. RIα co-immunoprecipitated with mTOR kinase, a major regulator of autophagy. Phosphorylated-mTOR levels and mTOR activity were dramatically increased in *prkar1a*$^{-/-}$ mouse cells, and in HEK 293 cells with RIα levels reduced by siRNA. Finally, phosphorylated-mTOR levels and mTOR activity were increased in CNC cells and in PPNAD tissues. These data suggest that RIα deficiency decreases autophagy by the activation of mTOR, providing a molecular basis to autophagic deficiency in PPNAD.

INTRODUCTION

Inactivating mutations of the human *PRKAR1A* gene cause a multiple neoplasia and lentiginosis syndrome, Carney complex (CNC) (1). The most common manifestations are multiple skin macules, known as lentigines, and other pigmented lesions such as blue and compound nevi and primary pigmented nodular adrenocortical disease (PPNAD) (2). Heavily pigmented macromelanosomes account for the pigmentation in lentigines and the nevi; however, the increased pigmentation in PPNAD nodules is due to the accumulation of lipofuscin-like material (3,4). Macromelanosomes are thought to originate from defective melanosome autophagocytosis (5,6), whereas accumulation of lipofuscin is a hallmark of autophagic deficiency (7,8).

Autophagy is an evolutionarily conserved mechanism in all eukaryotes; its basic role is the bulk turnover of long-lived proteins and cytoplasmic organelles. During the process of autophagy, portions of the cytosol, organelles or targeted cargo are sequestered in double membrane-bound vesicles (autophagosomes), which then fuse with lysosomes (or vacuoles in yeast) releasing the sequestered contents into the lumen for degradation by resident hydrolases (9,10). Inhibition of the target of rapamycin (TOR) kinase is a major prerequisite for starvation-induced autophagy in *Saccharomyces cerevisiae* (11), and it is required to control Atg1-dependent organization of protein complexes on the pre-autophagosomal membrane (12,13). Reduced TOR activity is also required for the maturation of the pre-autophagosomal vesicles into

*To whom correspondence should be addressed. Tel: +1 3014021010; Fax: +1 3014020078; Email: mavrakim@mail.nih.gov

Published by Oxford University Press.

autophagic vacuoles by increasing the expression of autophagic specific genes such as *ATG8* (14).

Both in yeast and higher eukaryotes, mTOR signaling plays a key role in various processes including protein translation, ribosome biogenesis, actin organization, mitochondrial oxygen consumption and oxidative capacity, metabolism, transcription of several nutrient- and stress-responsive factors and autophagy (15). The best studied targets of mTOR in mammalian cells are the translation regulators S6K1 and 4E-BP1. Phosphorylation of these targets by mTOR has provided a possible mechanism by which nutrient deprivation affects protein translation. However, no evidence indicates that mTOR affects autophagosome biogenesis and/or autophagic activity through phosphorylation of S6K1 or 4EBP1. In yeast, TOR negatively controls autophagy via inhibition of the protein kinase ATG1; however, the mammalian homolog of ATG1 has not yet been identified.

The human *PRKAR1A* gene encodes the regulatory subunit 1-alpha (RIα) of the cAMP-dependent protein kinase A (PKA) holoenzyme. Phosphorylation mediated by the cAMP/PKA signaling pathway can be elicited by various physiological ligands in cells and is critically involved in the regulation of metabolism, cell proliferation, differentiation and apoptosis (16). PKA exists as a tetrameric holoenzyme consisting essentially of two dimers: one composed of regulatory subunits, and the other of two inactive catalytic subunits (17). Cooperative binding of two cAMP molecules to each regulatory subunit results in dissociation and the consequent release (activation) of the two catalytic subunits. There are four genes encoding the different regulatory subunits (RIα, RIβ, RIIα, RIIβ) and three genes encoding the catalytic subunits Cα, Cβ and Cγ (18). RIα, RIIα and Cα are ubiquitously expressed, whereas the rest of these genes have tissue-specific expression (19). The best known function of the R subunits *in vitro* is inhibition of the C subunit kinase activity.

The pathological characteristics of CNC indicative of an autophagy deficiency, together with the role of the *PRKAR1A*-homolog *bcy1* in yeast autophagy, led us to investigate mTOR in human PPNAD tissues bearing inactivating *PRKAR1A* mutations. Complete *PRKAR1A* loss, as indicated by the loss of heterozygosity (LOH) and the corresponding normal allele in these tissues, was associated with the accumulation of autophagic substrates in the adenomatous nodules compared with the surrounding (hemizygous for *PRKAR1A*) normal adrenocortical cells. We then investigated the intracellular distribution of RIα and its association with mTOR kinase: fluorescently tagged RIα was found to associate with LC3-labeled autophagosomes. Accordingly, the number of LC3-labeled autophagosomes was significantly reduced in *prkar1a*$^{-/-}$ mouse embryonic fibroblasts (MEFs), which were devoid of any RIα protein. In biochemical assays, RIα was found to interact with mTOR and affect significantly its kinase activity. Downregulation of RIα in HEK293 cells increased phosphorylation of mTOR and mTOR kinase activity. Finally, PPNAD tissues with *PRKAR1A* mutations showed increased mTOR phosphorylation and mTOR activity. Altogether, our data suggest that indeed RIα and mTOR are involved in a common pathway regulating mammalian autophagy.

RESULTS AND DISCUSSION

PRKAR1A-null PPNAD tissues showed lipofuscin accumulation

Transverse sections of PPNAD tissues from patients with the 478delTG *PRKAR1A*-inactivating mutation (1) showed increased lipofuscin in the pigmented nodules when stained with Ziehl–Neelsen stain, which is specific for lipofuscin (3,4) (Fig. 1A). The pigmented nodules in these experiments were dissected using laser-capture microdissection (LCM) (Fig. 1B, upper panel), and DNA was isolated from these nodules, as well as from blood and total adrenoglandular tissue homogenates. LOH and, specifically, loss of the wild-type *PRKAR1A* allele were evident only in the adenoma cells that constituted the pigmented nodules (Fig. 1B, bottom panel). Lipofuscin accumulation is a hallmark of autophagic deficiency (7,8). Thus, our observation that lipofuscin accumulated only in the cells lacking both *PRKAR1A* alleles (making them devoid of any RIα protein) suggested a potential role of RIα in the regulation of autophagy.

EGFP-RIα localized on late endosomes and autophagosomes

To determine the subcellular localization of RIα, we expressed PRKAR1A (RIα) tagged with green fluorescent protein (EGFP, see Materials and Methods) in a variety of cell types (HeLa, MNT-1, NRK, COS-7, MEF) and observed its distribution in living and fixed cells. The tagged protein showed a diffuse cytosolic pool but was also found on spot-like structures scattered throughout the cell, with a pronounced perinuclear accumulation in most cells (Fig. 1C, EGFP-RIα). To ensure that the observed spot-like structures were not non-specific aggregates formed by the presence of EGFP, we also transfected cells with RIα tagged with HA and immunostained using anti-HA antibodies. HA-RIα displayed a pattern identical to the one observed in EGFP-RIα-transfected cells (Fig. 1C, HA-RIα). To further explore the nature of the spot-like structures and to determine if RIα molecules are immobilized on these structures, we performed fluorescence recovery after photobleaching (FRAP) experiments in cells expressing EGFP-RIα (20). A single spot-like structure was photobleached using a high-intensity laser beam, abolishing EGFP fluorescence. Low-power imaging was then used to assess fluorescence recovery into the photobleached region. A rapid and complete recovery of EGFP-RIα fluorescence was observed (Fig. 1D), indicating that EGFP-RIα molecules readily move on and off the structures, exchanging with a cytosolic pool of the protein.

To further investigate the subcellular localization of EGFP-RIα, we imaged EGFP-RIα in the presence of various organelle markers, either by immunostaining or in living cells co-transfected with different organelle markers. PKA regulatory subunit RIIβ has been shown to target PKA to the Golgi complex (21), so we began by looking at the potential association of EGFP-RIα with the Golgi complex. Toward this end, we visualized the Golgi stack using GalT-CFP, the *trans*-Golgi network using anti-TGN46 antibodies, the Golgi matrix using anti-GM130 antibodies and the ER-to-Golgi intermediate compartment using p58-CFP (see Materials and Methods). No colocalization of EGFP-RIα with any of these

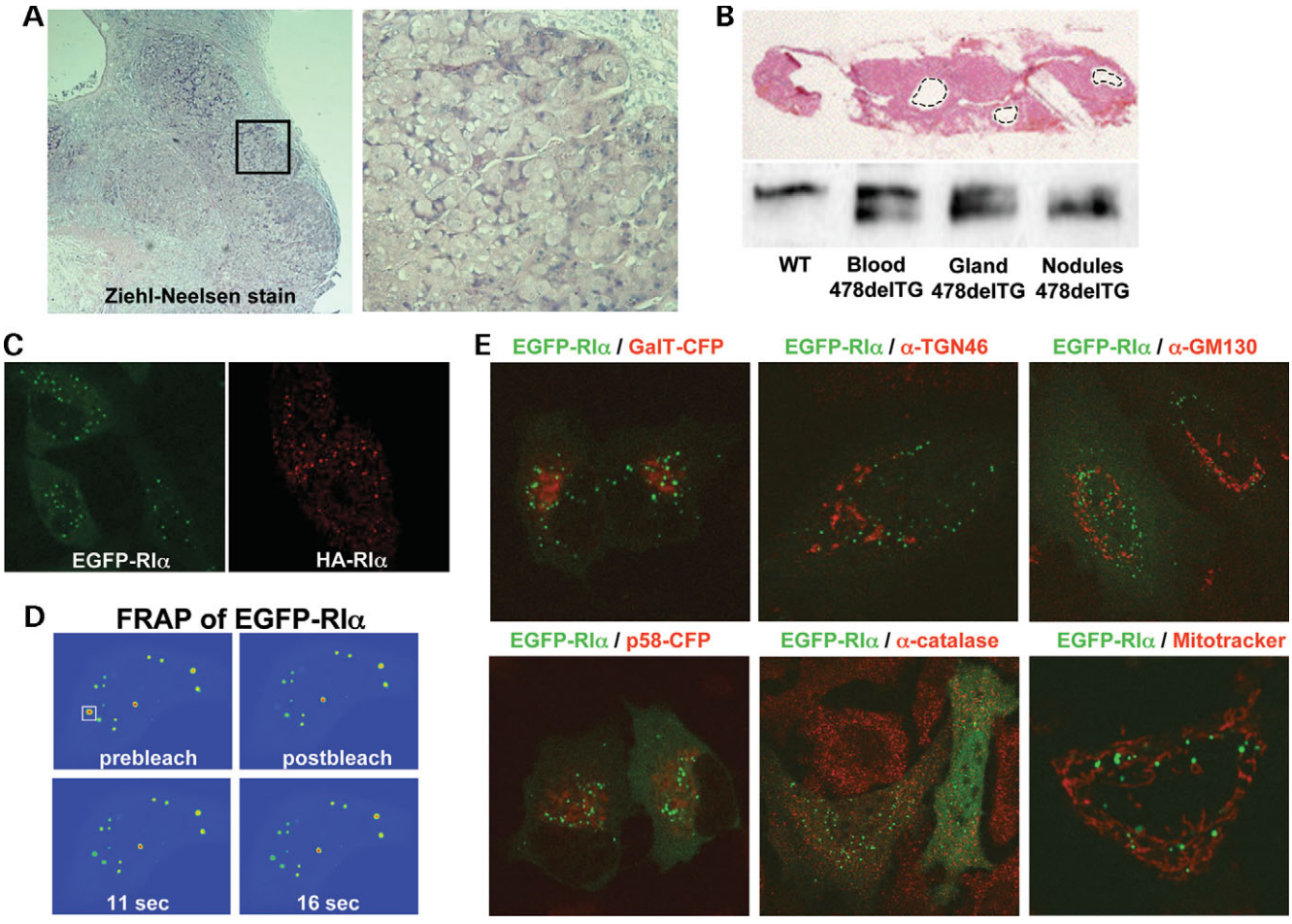

Figure 1. PPNAD caused by *PRKAR1A*-inactivating mutations is associated with lipofuscin accumulation in the nodular regions of the tissue. EGFP-RIα localized in the cytosol and on spot-like structures. Spot-like EGFP-RIα readily exchanged with the cytosolic pool of the protein and was not associated with Golgi, mitochondria or peroxisomes. (**A**) A PPNAD adrenal gland was stained with Ziehl–Neelsen-specific stain for lipofuscin (see Materials and Methods). A transverse section of the gland is shown to indicate lipofuscin accumulation in the pigmented nodules (left panel). The image on the right is a magnification of the black outlined rectangle in the image on the left. (**B**) Pigmented nodules in a PPNAD tissue were dissected using LCM (black dashed outlines, upper panel). Nodular DNA was prepared as described in *Materials and Methods* and used for PCR using the polymorphic marker *GATA1E12*, which cosegregated with the disease (1) in the family of the patient (bottom panel, nodules). PCR was also performed on lymphocyte DNA from the unaffected father (WT), lymphocyte DNA from the affected daughter (blood) and total tumor DNA (gland). The absence of the band segregating with the wild-type *PRKAR1A* allele indicated LOH only in the nodular cells. (**C**) EGFP-RIα exhibited a cytosolic and spot-like distribution in transiently transfected HeLa cells (left panel). The same distribution was observed in HeLa cells transiently transfected with HA-RIα (right panel), indicating that the spot-like distribution was not due to non-specific aggregation of EGFP. (**D**) EGFP-RIα on spot-like structures readily exchanged with the cytosolic pool of the protein as determined by FRAP. A small ROI (white outlined rectangle) encompassing an EGFP-RIα spot was photobleached and fluorescence recovery was monitored; EGFP-RIα fluorescence significantly recovered within seconds of photobleaching. (**E**) HeLa cells were transiently transfected with EGFP-RIα and then processed for immunostaining for peroxisomes (α-catalase), the Golgi matrix (α-GM130) and the *trans*-Golgi network (α-TGN46). Cells were co-transfected with p58-CFP to visualize the ER-to-Golgi intermediate compartment and with GalT-CFP to visualize the Golgi stack. For mitochondria staining, cells were incubated with Mitotracker before fixation (see Materials and Methods). EGFP-RIα spots did not associate with any of these compartments.

compartments was observed (Fig. 1E). We also imaged EGFP-RIα in the presence of a peroxisomal marker (anti-catalase) and a mitochondrial marker (Mitotracker), but no colocalization was observed (Fig. 1E).

We next investigated the potential association of RIα with endosomal compartments of the cell. For this, we imaged Venus-RIα coexpressed with Cerulean-tagged Rab5 (marking early endosomes) (22), Rab7 (marking lysosomes) or Rab9 (marking late endosomes) (23). Although no association of RIα with Rab5-positive endosomes was observed (data not shown), Venus-RIα was associated with a subset of Rab7- and Rab9-positive endosomes (Fig. 2A). In time-lapse sequences in living cells co-transfected with Venus-RIα and Cerulean-Rab9, Venus-RIα-positive spots were often seen to associate and move together with Cerulean-Rab9-positive endosomes (Fig. 2B). Venus-RIα was also associated with Cerulean-Rab7-positive endosomes, and when we selectively photobleached the Venus-RIα pool on these endosomes, it rapidly recovered, again indicating a dynamic exchange of Venus-RIα molecules on the endosomes with the cytosolic pool of RIα (Fig. 2C).

Rab7 is a small GTPase involved in lysosome biogenesis (24) and maturation of late autophagic compartments (25–27). Hence, our observation that RIα-containing structures were positive for Rab7 raised the question of whether these

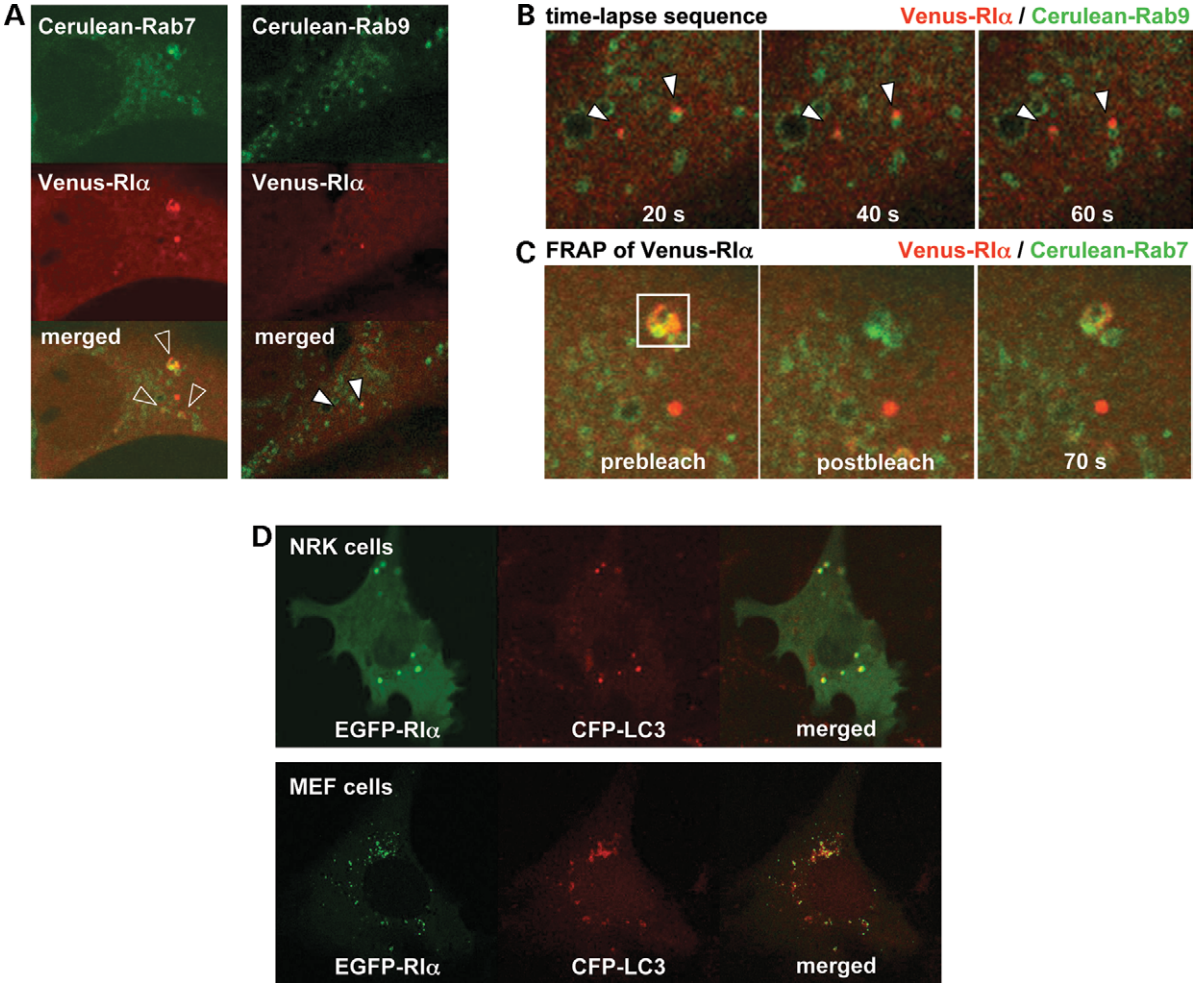

Figure 2. EGFP-RIα spots associated with late endosomes and autophagosomes. (**A**–**C**) HeLa cells were co-transfected with Venus-RIα and Cerulean-Rab7 or Cerulean-Rab9 to visualize late endosomes. Venus-RIα spots were often seen to associate and move with Rab7-positive endosomes (A, empty arrowheads) or Rab9-positive endosomes (A, white arrowheads). A time-lapse sequence is shown in (B), where Venus-RIα spots associated with Rab9-positive endosomes moved with the latter over time (white arrowheads). In a FRAP experiment (C), Venus-RIα, which was associated with Rab7-positive endosomes (white outlined rectangle) was selectively photobleached to show fast recovery of the RIα pool on the Rab7-positive endosome. (**D**) NRK or MEF cells were co-transfected with EGFP-RIα and CFP-LC3 to visualize autophagosomes. Representative confocal images are shown to demonstrate that the majority of EGFP-RIα spots associated with LC3-positive autophagosomes.

structures represented autophagosomes. To investigate this further, we co-transfected EGFP-RIα-expressing cells with CFP-LC3, a protein that has been shown to specifically associate with membranes of maturating autophagosomes (27–29). Representative confocal images are shown in Figure 2D. Virtually all the RIα-expressing structures were labeled with CFP-LC3. This suggested that RIα resides on autophagosomes, where it potentially functions.

The number of autophagosomes is reduced in *prkar1a*$^{-/-}$ MEFs

To investigate a possible role of RIα on autophagosomes, we examined the CFP-LC3 distribution in *prkar1a*$^{+/+}$ and *prkar1a*$^{-/-}$ MEF cell lines (see Materials and Methods), which express or do not express RIα. Although *prkar1a*$^{+/+}$ MEFs showed a pronounced perinuclear accumulation of LC3-labeled autophagosomes, in *prkar1a*$^{-/-}$ MEFs, there were a remarkably decreased number of LC3-labeled autophagosomes; in addition, there was an increased cytosolic and nuclear pool of LC3 (Fig. 3A). To quantify the observed differences, autophagosomes were counted in each cell line (Fig. 3B). A statistically significant difference in the number of autophagosomes was observed, with *prkar1a*$^{+/+}$ cells having on average 18 autophagosomes per cell compared with ~3 in *prkar1a*$^{-/-}$ cells that lack RIα.

Riα and mTOR co-immunoprecipitated and phosphorylated-mTOR levels and mTOR activities were increased in cells with low RIα levels

Given that RIα associates with autophagosomes and that there is a reduced number of autophagosomes in *prkar1a*$^{-/-}$ cells, which lack RIα (Figs 2D and 3), we next investigated whether

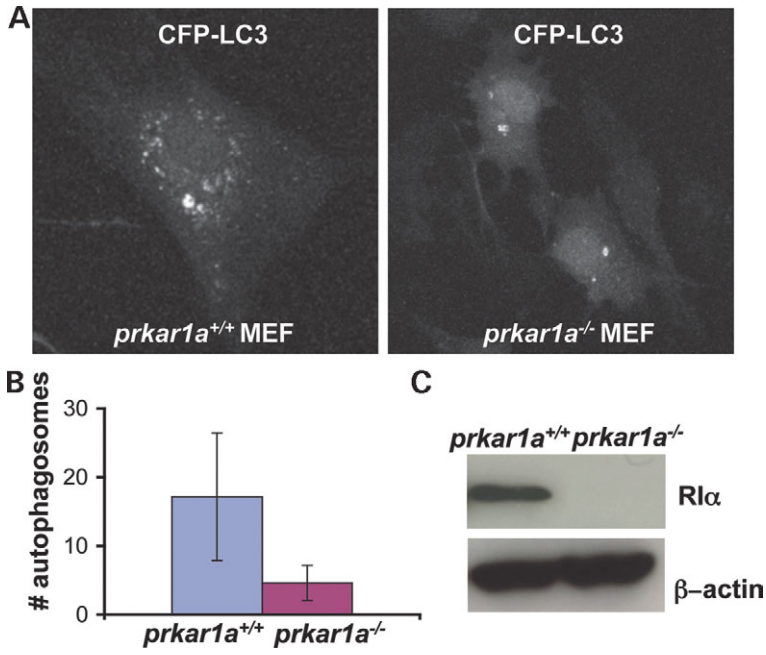

Figure 3. The number of autophagosomes is reduced in *prkar1a*$^{-/-}$ MEFs. Representative confocal images of *prkar1a*$^{+/+}$ MEFs and *prkar1a*$^{-/-}$ MEFs, transiently transfected with CFP-LC3 to visualize autophagosomes (**A**). CFP-LC3 accumulated on autophagosomes in *prkar1a*$^{+/+}$ MEFs (A, left panel), whereas it did so to a much lesser extent in *prkar1a*$^{-/-}$ MEFs, exhibiting a higher cytosolic and nuclear pool in the latter (A, right panel). For quantitation, both cell lines were optically sliced on a confocal microscope (see Materials and Methods) and then maximum intensity z-projections were generated for each cell to visualize all autophagosomes, which were then counted. The average number of autophagosomes in each cell line was plotted (**B**, shown as mean ± SD). Immunoblots showing RIα levels in each cell line are shown in (**C**), along with β-actin immunostaining as a protein-loading control.

RIα interacts with mTOR kinase in immunoprecipitation experiments. RIα was immunoprecipitated from HEK 293 cells transfected with HA-RIα, and the pellet was then immunoblotted for mTOR. Notably, mTOR was seen co-precipitating with RIα (Fig. 4A, left panel). Inversely, when endogenous mTOR was immunoprecipitated and the pellet immunoblotted for RIα, RIα was found to co-precipitate with mTOR (Fig. 4A, right panel). The data thus suggested that a pool of RIα and a pool of mTOR molecules form a complex within the cell.

To further investigate the connection between mTOR and RIα, we measured total protein levels of mTOR, levels of phosphorylated mTOR ('phospho-mTOR') and levels of mTOR activity (see Materials and Methods) in cells with experimentally altered amounts of RIα protein. Phosphorylated-mTOR levels were assessed using a phospho-mTOR antibody specific for Ser2448. We utilized cells that were transfected with pcDNA3.1 ('mock'), pcDNA3.1-RIα (to overexpress RIα) or RIα siRNA (to silence RIα). Additionally, *prkar1a*$^{+/+}$ and *prkar1a*$^{-/-}$ MEFs were used. In each cell condition, RIα, mTOR and phosphorylated-mTOR levels were assayed by immunoblotting (Fig. 4B and C). In *prkar1a*$^{-/-}$ MEFs and in cells transfected with RIα siRNA, a dramatic increase in phosphorylated-mTOR levels in cells with low RIα levels was observed (Fig. 4D). Total mTOR levels were not different in these experimental groups (Fig. 4C). This observation suggested that RIα is involved in the mechanism of mTOR phosphorylation. We then measured mTOR activity under the earlier-mentioned conditions and found that, in *prkar1a*$^{-/-}$ MEFs and in cells transfected with RIα siRNA, mTOR activity was also dramatically increased in cells with low RIα levels (Fig. 4E). We also treated cells with rapamycin, one of the drugs commonly used to inhibit the mTOR kinase, and looked at the number of autophagosomes, mTOR phosphorylation and activity, but both HEK 293 and wild-type MEF cells were not responsive to rapamycin (data not shown). In cultured cells, therefore, reduced RIα level (by siRNA or in *prkar1a*$^{-/-}$ cells) is correlated with (1) increased phosphorylation of mTOR (2) increased mTOR activity and (3) reduced autophagic vacuole formation.

PPNAD tissues with *PRKAR1A* mutations show increased phosphorylated-mTOR staining and mTOR activity

To determine whether a similar relationship among RIα levels, mTOR activity and autophagic vacuole formation occurs in pigmented nodules of PPNAD patients, we performed immunohistochemistry (IHC) on these structures using anti-phosphorylated-mTOR antibodies (see Materials and Methods). In normal tissues, as well in tissues from other adrenocortical tumors, in which both wild-type *PRKAR1A* alleles are present, phospho-mTOR staining was not prominent (Fig. 5A). However, in tissues from four PPNAD patients (each caused by a different *PRKAR1A*-inactivating mutation), phospho-mTOR staining in the nodules was dramatically increased (Fig. 5A, CAR002.02, CAR025.01, CAR047.01, CAR555.03). mTOR activity was also assayed in microscopically dissected nodular tissue from the same patients and significantly increased mTOR activity was found

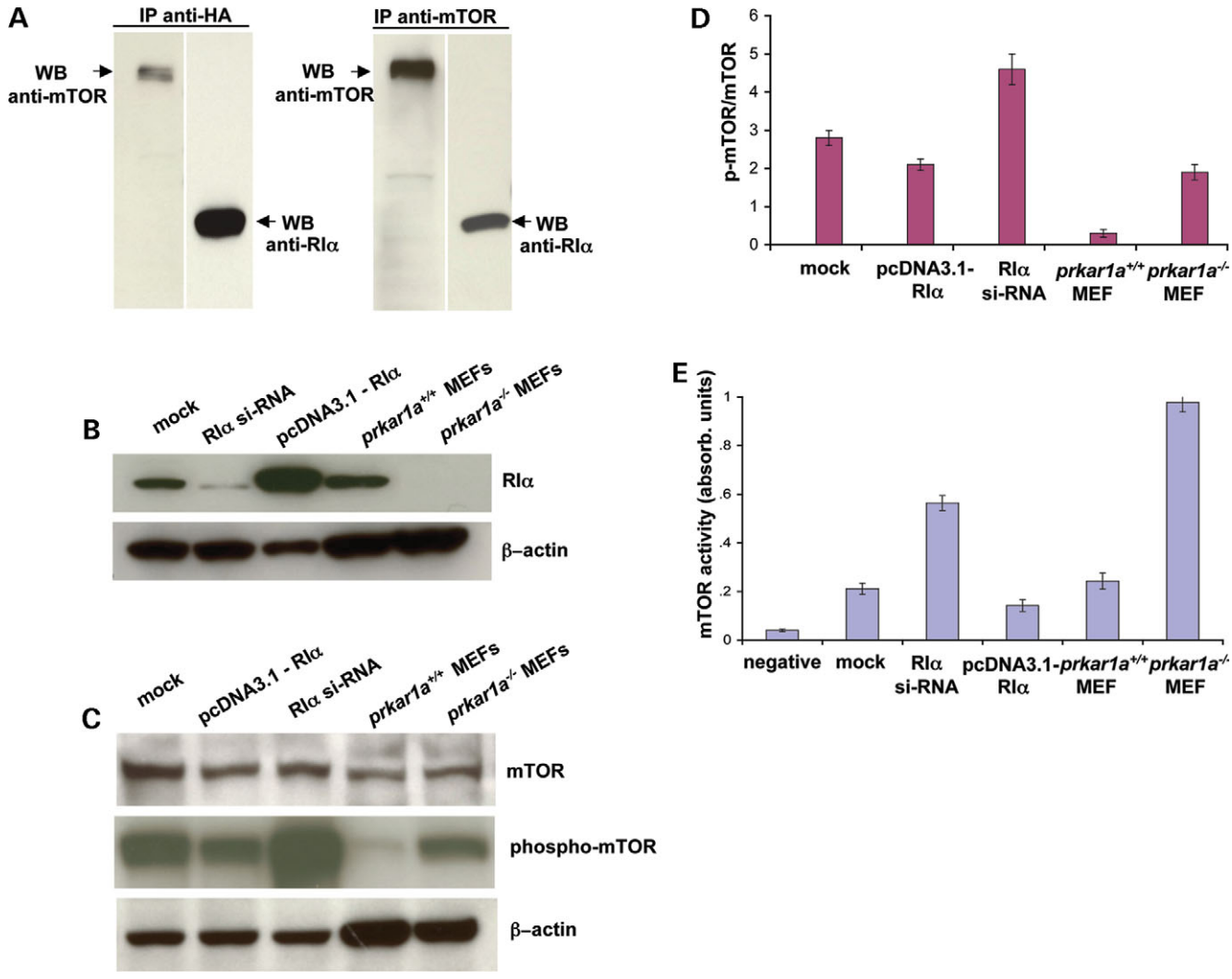

Figure 4. RIα and mTOR co-immunoprecipitated; phosphorylated-mTOR levels and mTOR activity were found increased in cells with low RIα levels. (**A**) HEK 293 cells were transfected with HA-RIα, and RIα was immunoprecipitated with α-HA antibodies. The pellet was then immunoblotted against mTOR and RIα, and mTOR was found to co-immunoprecipitate with RIα (left panel). Inversely, when endogenous mTOR was immunoprecipitated in HEK 293 cells and the pellet immunoblotted against mTOR and RIα, RIα was found to co-immunoprecipitate with mTOR (right panel). (**B**) Cells were transfected with pcDNA3.1 (mock), pcDNA3.1-RIα to overexpress RIα or RIα siRNA to silence RIα, and RIα levels under all conditions were assayed by immunoblotting. RIα levels were also assayed in wild-type ($prkar1a^{+/+}$) and $prkar1a^{-/-}$ MEFs. β-actin was used as a protein-loading control. (**C**) mTOR and phosphorylated-mTOR levels were measured by immunoblotting in cells with experimentally altered RIα levels (B). Phosphorylated-mTOR levels were assessed using a phospho-mTOR antibody specific for Ser2448. β-actin was used as a protein-loading control. (**D**) mTOR and phosphorylated-mTOR immunoblots shown in (C) were quantified by densitometry and the phospho-mTOR/mTOR ratio plotted for each condition. There was no significant difference in total mTOR levels but the phospho-mTOR/mTOR ratio was highest in $prkar1a^{-/-}$ cells and cells where RIα was silenced by RNAi, indicating that RIα is involved in mTOR phosphorylation. (**E**) mTOR activity was measured in the absence of any lysate (negative), cells transfected with pcDNA3.1 (mock), pcDNA3.1-RIα and RIα siRNA and wild-type and $prkar1a^{-/-}$ MEFs. mTOR activity was highest in $prkar1a^{-/-}$ MEFs and cells where RIα was silenced by RNAi, as was the phospho-mTOR/mTOR ratio under these conditions, indicating that mTOR activity is highly correlated with phosphorylation of mTOR at Ser2448.

compared with the perinodular tissue (Fig. 5B). Since the pigmented nodules in the PPNAD patients have reduced autophagic activity (assessed by lipofuscin accumulation), the data support a role for RIα in regulating mammalian autophagy through the mTOR kinase.

These findings provide a basis for explaining the cellular phenotype of a primary adrenocortical hyperplasia (PPNAD). The hallmark of this disorder, lipofuscin accumulation, would appear to result from autophagy deficiency caused by increased mTOR phosphorylation and activity in response to RIα depletion. Because dysregulation of mTOR activity has been implicated in the pathogenesis of several hamartoma syndromes (30), including those caused by the tuberous sclerosis complex, the Peutz–Jeghers, LEOPARD and the PTEN-related syndromes (Cowden disease, Proteus syndrome, Lhermitte–Duclos disease), it is possible that RIα is involved in alterations in mTOR signaling in each of these hamartoma syndromes, as our study demonstrates for CNC.

Previously, the PKA signaling system was not directly linked to the regulation of mTOR or autophagy in mammalian cells, although an interaction was speculated on the basis of studies on *S. cerevisiae* showing a regulatory role of PKA

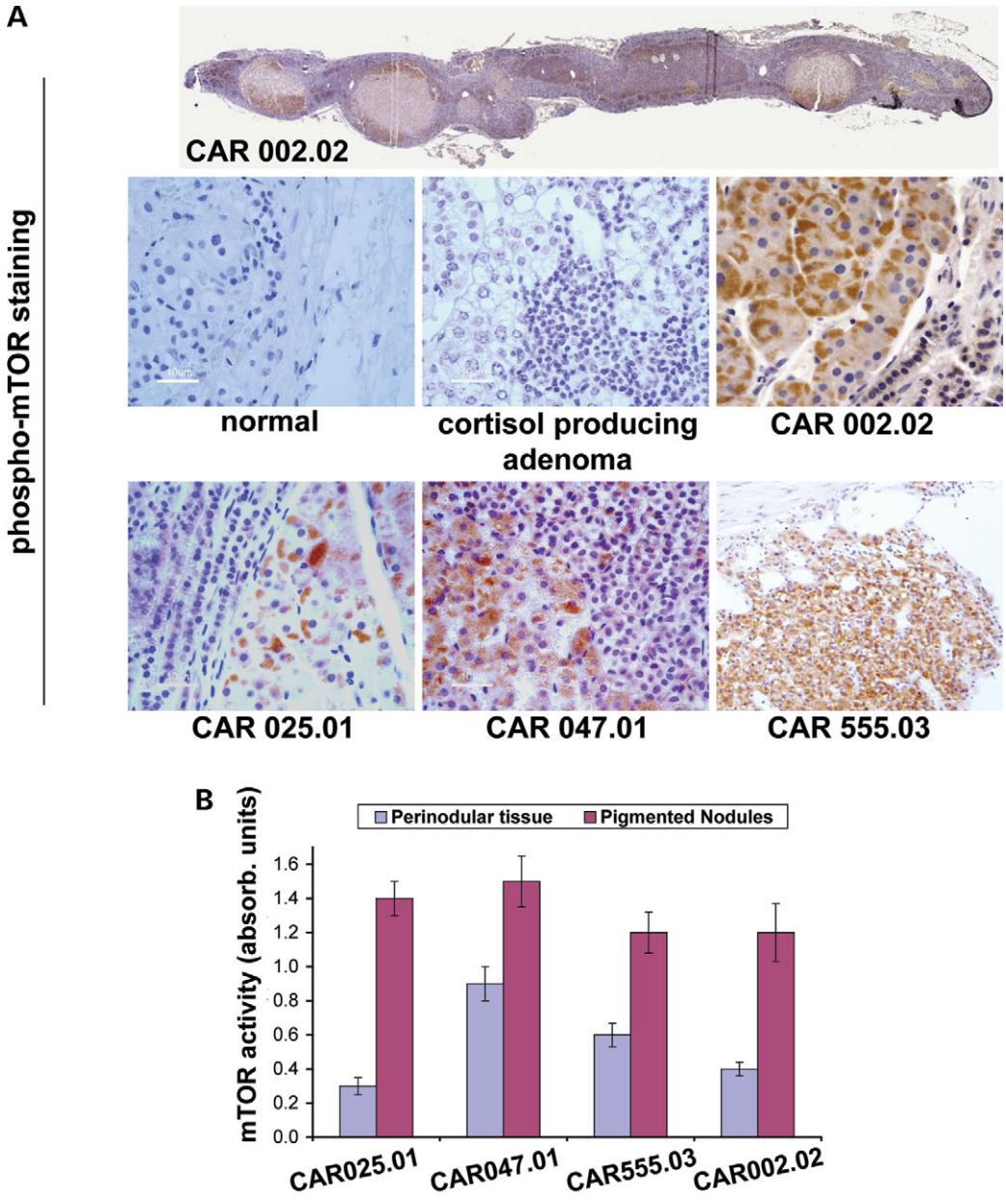

Figure 5. PPNAD tissues with mutations in *PRKAR1A* show increased phosphorylated-mTOR staining and increased mTOR activity. (**A**) Phosphorylated-mTOR IHC (see Materials and Methods) was performed on adrenal glands from healthy individuals ('normal'), PPNAD patients (CAR002.02, CAR025.01, CAR047.01, CAR555.03) or patients with other adrenocortical tumors (a cortisol-producing adenoma in this case). Phosphorylated-mTOR staining was dramatically increased in PPNAD nodules compared with normal tissue or nodules from cortisol-producing adenoma tissue. (**B**) mTOR activity was measured in microscopically dissected PPNAD nodules (see Materials and Methods). mTOR activity was found to be dramatically increased compared with the perinodular tissue. Increased mTOR activity and increased phosphorylated-mTOR levels, together with lipofuscin accumulation and loss-of-heterozygosity at the *PRKAR1A* locus only in the pigmented nodules, strongly suggested that mTOR and RIα are indeed involved in a common pathway regulating autophagy.

signaling in autophagy (30,31). Indeed, in a recent proteomics study, ATG1, ATG13 and ATG18 (components of the yeast autophagic machinery) were identified as potential PKA phosphorylation substrates (32). In a different study, Bcy1 (yeast homolog of RIα)-mutant yeast strains displayed constitutively high PKA activity and did not tolerate nutrient deprivation due to defective autophagy (33). These effects were not mediated by increased PKA catalytic activity since in *BCY1*-null cells containing a mutated *TPK1* gene and deleted of *TPK2* and *TPK3* (*TPK1*, *TPK2* and *TPK3* are the catalytic subunits of yeast PKA), PKA activity was not excessively elevated (34). However, these cells were not responsive to starvation-induced autophagy, indicating Bcy1 is important for normal autophagy regardless of cAMP-dependent kinase activity.

Our study suggests that RIα and the mTOR kinase are mechanistically linked in regulating autophagy, with RIα deficiency decreasing autophagy by the activation of mTOR. Further work is needed to understand how this occurs. One

possibility relates to the fact that RIα has a kinase interaction domain that binds to the catalytic subunit of PKA. Because mTOR is a serine/threonine kinase (like PKA), the interaction of RIα with mTOR may block mTOR phosphorylation. In this model, RIα would be required to maintain phosphorylated levels of mTOR at low levels, as increased phosphorylation of mTOR blocks autophagy. Another possible model is that RIα forms a complex with a phosphatase and an mTOR. This is consistent with current literature supporting a role for phosphatases in controlling the phosphorylation status of mTOR (30). In this scenario, RIα would sequester a phosphatase in an RIα–mTOR–phosphatase complex and thereby control mTOR phosphorylation.

MATERIALS AND METHODS

Analysis of allelic losses in microdissected PPNAD tissues

LOH analysis was performed as has been previously described (1), using the polymorphic marker *GATA1E12*. The PCR reactions were performed on lymphocyte DNA from the unaffected father, lymphocyte DNA from the affected daughter, total tumor DNA and DNA from LCM-obtained PPNAD nodular tissue. For LCM, histological sections were prepared from formalin-fixed paraffin-embedded tissue and were stained with hematoxylin and eosin for microscopic evaluation. From these slides, the nodular areas were identified. Laser-assisted microdissection of the nodular epithelium was performed on the unstained sections using a PixCell II laser capture microdissection system (Arcturus Engineering, Mountain View, CA, USA), as previously described (35). Approximately 2000 cells were microdissected from the 5 μm histological sections. After microdissection, the cells were inserted into an Eppendorf tube dewaxed, rehydrated and finally incubated with digestion buffer (50 μl buffer containing 0.04% Proteinase K, 10 mM Tris–HCl pH 8.0, 1 mM EDTA and 1% Tween-20) at 37°C overnight. The reactions were terminated by heating to 95°C for 10 min to inactivate the proteinase K and used directly for PCR.

Identification of lipofuscin in PPNAD

Ziehl–Neelsen stain for lipofuscin was performed on formalin-fixed paraffin-embedded PPNAD adrenal tumors, as has been previously described (3). Five micrometer paraffin sections from PPNAD tumors were mounted on adhesive-coated slides. After dewaxing with xylenes and rehydration in a graded series of ethanol, warm carbol-fuchsin solution was applied to the section slides for 5 min at 45°C. Destaining was done with 1% concentrated hydrochloric acid in 70% ethanol (vol/vol) for 5 min at room temperature. No counterstain was used. The glycerol-mounted sections were observed with a Nikon Optiphoto microscope with differential interference-contrast (Nomarski) optics before and after acid-fast staining.

Cell cultures

HeLa cells were cultured in Dulbecco's modified Eagle's medium supplemented with 10% heat-inactivated fetal bovine serum, penicillin and streptomycin under 5% CO_2. Wild-type (*prkar1a*$^{+/+}$) primary MEFs were isolated from six day-10 mouse embryos of C57BL6xSJL mixed background. *prkar1a*$^{-/-}$ MEF cells were kindly given to us by Dr L. Kirschner (Ohio State University, Columbus, OH) and they have been described elsewhere (36); these cells have also been created from mice of the same mixed genetic background. HEK293 cells were used for immunoblotting and immunoprecipitation experiments.

Antibodies and expression constructs

The following antibodies were used for immunofluorescence: rabbit anti-catalase (1:500) from Calbiochem (cat. no. 219010), mouse anti-GM130 (1:50) from Transduction Laboratories (cat. no. G65120), sheep anti-TGN46 (1:1000) from Serotec (cat. no. AHP500), AF546-conjugated goat anti-mouse (1:1000) from Molecular Probes, AF546-conjugated goat anti-rabbit (1:1000) from Molecular Probes and Cy3-conjugated donkey anti-sheep (1:1000) from Jackson Immunoresearch Laboratories. For immunoblotting, an anti-RIα monoclonal antibody (1:500) was obtained from BD Transduction Laboratories (cat. no. 610610), an anti-mTOR polyclonal antibody (1:2000) from Abcam (cat. no. ab2833-50) and rabbit polyclonal anti-Phospho-mTOR (Ser2448) (1:1000) from Cell Signaling Technologies (cat. no 2971). The following conjugated antibodies were used for immunoprecipitations: agarose-immobilized anti-HA high-affinity rat monoclonal antibody (clone 3F10) from Roche (cat. no. 11815016001) at 50μL/100 μg of protein and agarose immobilized rabbit polyclonal anti-mTOR (4 μg/200 μg of total protein) from Abcam (cat. no. ab19207-100). For IHC, a rabbit mAb anti-Phospho-mTOR (Ser2448) (49F9) was obtained from Cell Signaling Technologies (cat. no. 2976) and used at 1:50 dilution. GalT-CFP, p58-CFP and CFP-LC3 constructs have been described previously (37,38). ECFP-Rab7 and EGFP-Rab9 constructs were a gift from S. Pfeffer (Stanford University School of Medicine, CA). ECFP and EGFP were then replaced by Cerulean from the pCerulean-C1 plasmid using *Age*I and *Bsr*GI restriction sites to generate Cerulean-Rab7 and Cerulean-Rab9.

Cloning of RIα constructs

pcDNA3.1-HA-RIα was prepared by subcloning a *Hin*dIII/*Xho*I fragment of the HA-tagged human PRKARIA cDNA from pREP4-HA-RIA (39), which was kindly given to us from Dr J. Bertherat (Hospital Cochin, Paris, France). For generation of pcDNA3.1-RIα, the *PRKAR1A* ORF was PCR-amplified from pREP4-HA-RIα using primers flanked by *Bam*HI and *Sal*I sites (AAGGATCCACCATGGAGTCT GGCAGTACCG and ACAGTCGACTCAGACAGACAGT GACACAAAAC). After digestion with *Bam*HI and *Sal*I, the fragment was ligated in *Bam*HI/*Xho*I-digested pcDNA3.1(−). For generation of pEGFP-RIα and Venus-RIα, the PRKAR1 A ORF was PCR-amplified with primers flanked by *Xho*I/*Bam*HI sites (TATCTCGAGAGTCTGGCAGTACCGCCA and GTGGATCCTCAGACAGACAGTGACACAAAAC). After digestion with *Xho*I and *Bam*HI, the fragment was

ligated in frame with *Xho*I/*Bam*HI-digested pEGFP-C1 and Venus-C1.

mTOR and RIα immunoprecipitation and immunoblotting

For HA-RIα and endogenous mTOR co-immunoprecipitations, 6×10^6 HEK293T cells growing in 175 cm^2 flasks were transfected with 40 μg of pcDNA3.1-HA-RIα using Lipofectamine 2000 (Invitrogen). Forty-eight hours post-transfection, the cells were collected with cold PBS/EDTA and lysed with 2 ml of lysis buffer (25 mM HEPES pH 7.5, 150 mM NaCl, 2 mM EDTA, 0.4% CHAPS, 10 mM glycerolphosphate, 25 mM NaF, 1 mM sodium orthovanadate and a complete protease inhibitor cocktail (Roche). After a brief sonication, the lysates were clarified by centrifugation at 16 000*g* for 20 min. One microgram of total protein was incubated overnight with either 100 μl of anti-HA or anti-mTOR agarose beads. Captured immunoprecipitates were washed three times with lysis buffer and subjected to western blot analysis for RIα and mTOR.

For immunoblotting, equivalent amounts of protein were separated using SDS–PAGE and then transferred to a nitrocellulose membrane. Membranes were blocked with blocking buffer (TBST-5% milk) for 1 h, probed with primary antibodies for 2 h and then incubated with the HRP-conjugated secondary antibody for 1 h. Antibody binding was detected by enhanced chemiluminescence (Amersham). Density for each band was analyzed using a densitometer. Equal protein loading was confirmed by probing β-actin. Values obtained for phosphorylated mTOR were normalized to total mTOR density. For immunoprecipitation, 300 μg of lysate proteins were immunoprecipitated overnight with the primary antibody of interest along with protein A agarose beads in lysis buffer and then used for kinase activity assays.

mTOR activity measurement

mTOR activity in tissues and cells were measured using a commercially available Elisa kit (Calbiochem, cat# CBA055) according to instructions by the manufacturer. This ELISA-based activity assay utilizes a p70S6K-GST fusion protein as a specific mTOR substrate. The mTOR substrate is first bound to a solid support, and mTOR-containing sample is incubated with ATP in the wells of a glutathione-coated 96-well plate where active mTOR phosphorylates p70S6K at Thr389. The phosphorylated substrate is detected with Anti-p70S6K-T389 antibody, followed by detection with HRP-antibody conjugate and TMB substrate. Transfected cells or micro-dissected PPNAD tumors were lysed by sonication in lysis buffer (50 mM Tris–HCl pH 7.4, 100 mM NaCl, 50 mM β-glycerophosphate, 10% glycerol, 1% Tween-20, 1 mM EDTA, 20 nM microcystin-LR, 25 mM NaF and a cocktail of protease inhibitors). The lysates were clarified by centrifugation (16 000*g* for 20 min) and total protein concentration was adjusted to 3 mg/ml with lysis buffer; 0.5 ml of the lysates were incubated for 2 h at 4°C with 25 μl of anti-mTOR agarose beads. The immunoprecipitates were washed twice with lysis buffer and twice with kinase buffer before incubation with the mTOR substrate.

IHC and immunofluorescence

IHC for phospho-mTOR on paraffin-embedded PPNAD tumors, normal adrenal and cortisol-producing adenomas was performed as previously described (40) using the citrate antigen retrieval method and TBST/BSA (50 mM Tris pH 7.5, 137 mM NaCl, 0.1% Tween-20, 1% IgG-free BSA) as the blocking and antibody diluent buffer.

For immunofluorescence, HeLa cells were grown on coverslips and fixed in 4% formalin (15 min), followed by blocking in 0.1% saponin, 1% BSA-PBS (10 min) and sequential incubations with the primary and secondary antibodies. Wash steps before and after antibody incubations were performed using 0.1% saponin and 1% BSA-PBS. Cells were washed in PBS and mounted on slides with Fluoromount-G (Southern Biotechnology Associates, Birmingham, AL) in preparation for microscopy. Mitochondria were visualized by staining with MitoTracker Deep Red 633 (Molecular probes) at a final concentration of 300 nM.

Fluorescence microscopy and photobleaching

For colocalization studies, cells were seeded overnight in Lab-TekTM chambers (Nalge Nunc, Rochester, NY) and cotransfected with the plasmids of interest, using Lipofectamine™ 2000 (Invitrogen). Confocal microscope images of cells 15–24 h post-transfection were captured on a Zeiss 510 or Zeiss ConfoCor-2 inverted microscope using the 413 nm line of a Kr laser with a 430–470 emission filter for Cerulean/GFP, the 488 nm line of an Ar laser with a 505–530 emission filter for EGFP, a 543 nm HeNe laser line with a 560-615 emission filter for Cy3/AF546 and a 633 nm HeNe laser line with a long-pass 650 emission filter for MitoTracker Deep Red 633. Images were captured with a Plan-Apochromat® 1.4 NA 63× oil immersion objective. Cells expressing both proteins were selected for z-sectioning. Z stacks were taken using a pinhole of 1 Airy unit for both channels. Images were analyzed with ImageJ and Zeiss Image Examiner software and prepared by Adobe Photoshop 7.0. FRAP was performed by photobleaching a small region of interest (ROI) and monitoring fluorescence recovery over time, as described previously (20,41).

Conflict of Interest statement. None declared.

REFERENCES

1. Kirschner, L.S., Carney, J.A., Pack, S.D., Taymans, S.E., Giatzakis, C., Cho, Y.S., Cho-Chung, Y.S. and Stratakis, C.A. (2000) Mutations of the gene encoding the protein kinase A type I-alpha regulatory subunit in patients with the Carney complex. *Nat. Genet.*, **26**, 89–92.
2. Stratakis, C.A. (2002) Mutations of the gene encoding the protein kinase A type I-alpha regulatory subunit (PRKAR1A) in patients with the 'complex of spotty skin pigmentation, myxomas, endocrine overactivity, and schwannomas' (Carney complex). *Ann. N.Y. Acad. Sci.*, **968**, 3–21.
3. Shenoy, B.V., Carpenter, P.C. and Carney, J.A. (1984) Bilateral primary pigmented nodular adrenocortical disease. Rare cause of the Cushing syndrome. *Am. J. Surg. Pathol.*, **8**, 335–344.
4. Carney, J.A. and Ferreiro, J.A. (1996) The epithelioid blue nevus. A multicentric familial tumor with important associations, including cardiac myxoma and psammomatous melanotic schwannoma. *Am. J. Surg. Pathol.*, **20**, 259–272.

5. Horikoshi, T., Jimbow, K. and Sugiyama, S. (1982) Comparison of macromelanosomes and autophagic giant melanosome complexes in nevocellular nevi, lentigo simplex and malignant melanoma. *J. Cutan. Pathol.*, **9**, 329–339.
6. Jimbow, K. and Horikoshi, T. (1982) The nature and significance of macromelanosomes in pigmented skin lesions: their morphological characteristics, specificity for their occurrence, and possible mechanisms for their formation. *Am. J. Dermatopathol.*, **4**, 413–420.
7. Stroikin, Y., Dalen, H., Loof, S. and Terman, A. (2004) Inhibition of autophagy with 3-methyladenine results in impaired turnover of lysosomes and accumulation of lipofuscin-like material. *Eur. J. Cell Biol.*, **83**, 583–590.
8. Brunk, U.T. and Terman, A. (2002) Lipofuscin: mechanisms of age-related accumulation and influence on cell function. *Free Radic. Biol. Med.*, **33**, 611–619.
9. Baba, M., Takeshige, K., Baba, N. and Ohsumi, Y. (1994) Ultrastructural analysis of the autophagic process in yeast: detection of autophagosomes and their characterization. *J. Cell Biol.*, **124**, 903–913.
10. Levine, B. and Klionsky, D.J. (2004) Development by self-digestion: molecular mechanisms and biological functions of autophagy. *Dev. Cell*, **6**, 463–477.
11. Noda, T. and Ohsumi, Y. (1998) Tor, a phosphatidylinositol kinase homologue, controls autophagy in yeast. *J. Biol. Chem.*, **273**, 3963–3966.
12. Kim, J., Huang, W.P., Stromhaug, P.E. and Klionsky, D.J. (2002) Convergence of multiple autophagy and cytoplasm to vacuole targeting components to a perivacuolar membrane compartment prior to *de novo* vesicle formation. *J. Biol. Chem.*, **277**, 763–773.
13. Suzuki, K., Kirisako, T., Kamada, Y., Mizushima, N., Noda, T. and Ohsumi, Y. (2001) The pre-autophagosomal structure organized by concerted functions of APG genes is essential for autophagosome formation. *Embo J.*, **20**, 5971–5981.
14. Abeliovich, H., Dunn, W.A., Jr, Kim, J. and Klionsky, D.J. (2000) Dissection of autophagosome biogenesis into distinct nucleation and expansion steps. *J. Cell Biol.*, **151**, 1025–1034.
15. Wullschleger, S., Loewith, R. and Hall, M.N. (2006) TOR signaling in growth and metabolism. *Cell*, **124**, 471–484.
16. Cohen, P. (2002) The origins of protein phosphorylation. *Nat. Cell Biol.*, **4**, E127–E130.
17. Reimann, E.M., Brostrom, C.O., Corbin, J.D., King, C.A. and Krebs, E.G. (1971) Separation of regulatory and catalytic subunits of the cyclic 3',5'-adenosine monophosphate-dependent protein kinase(s) of rabbit skeletal muscle. *Biochem. Biophys. Res. Commun.*, **42**, 187–194.
18. Foss, K.B., Landmark, B., Skalhegg, B.S., Tasken, K., Jellum, E., Hansson, V. and Jahnsen, T. (1994) Characterization of *in vitro*-translated human regulatory and catalytic subunits of cAMP-dependent protein kinases. *Eur. J. Biochem.*, **220**, 217–223.
19. Bossis, I., Voutetakis, A., Matyakhina, L., Pack, S., Abu-Asab, M., Bourdeau, I., Griffin, K.J., Courcoutsakis, N., Stergiopoulos, S., Batista, D. *et al*. (2004) A pleiomorphic GH pituitary adenoma from a Carney complex patient displays universal allelic loss at the protein kinase A regulatory subunit 1A (PRKARIA) locus. *J. Med. Genet.*, **41**, 596–600.
20. Lippincott-Schwartz, J. and Patterson, G.H. (2003) Development and use of fluorescent protein markers in living cells. *Science*, **300**, 87–91.
21. Nigg, E.A., Schafer, G., Hilz, H. and Eppenberger, H.M. (1985) Cyclic-AMP-dependent protein kinase type II is associated with the Golgi complex and with centrosomes. *Cell*, **41**, 1039–1051.
22. Rink, J., Ghigo, E., Kalaidzidis, Y. and Zerial, M. (2005) Rab conversion as a mechanism of progression from early to late endosomes. *Cell*, **122**, 735–749.
23. Soldati, T., Rancano, C., Geissler, H. and Pfeffer, S.R. (1995) Rab7 and Rab9 are recruited onto late endosomes by biochemically distinguishable processes. *J. Biol. Chem.*, **270**, 25541–25548.
24. Bucci, C., Thomsen, P., Nicoziani, P., McCarthy, J. and van Deurs, B. (2000) Rab7: a key to lysosome biogenesis. *Mol. Biol. Cell*, **11**, 467–480.
25. Jager, S., Bucci, C., Tanida, I., Ueno, T., Kominami, E., Saftig, P. and Eskelinen, E.L. (2004) Role for Rab7 in maturation of late autophagic vacuoles. *J. Cell Sci.*, **117**, 4837–4848.
26. Gutierrez, M.G., Munafo, D.B., Beron, W. and Colombo, M.I. (2004) Rab7 is required for the normal progression of the autophagic pathway in mammalian cells. *J. Cell Sci.*, **117**, 2687–2697.
27. Eskelinen, L. (2005) Maturation of autophagic vacuoles in mammalian cells. *Autophagy*, **1**, 1–10.
28. Kabeya, Y., Mizushima, N., Ueno, T., Yamamoto, A., Kirisako, T., Noda, T., Kominami, E., Ohsumi, Y. and Yoshimori, T. (2000) LC3, a mammalian homologue of yeast Apg8p, is localized in autophagosome membranes after processing. *Embo J.*, **19**, 5720–5728.
29. Bampton, E.T.W., Goemans, C.G., Niranjan, D., Mizushima, N. and Tolkovsky, A.M. (2005) The Dynamics of Autophagy Visualized in Live Cells. *Autophagy*, **1**, 23–36.
30. Inoki, K., Corradetti, M.N. and Guan, K.L. (2005) Dysregulation of the TSC-mTOR pathway in human disease. *Nat. Genet.*, **37**, 19–24.
31. Bauer, A.J. and Stratakis, C.A. (2005) The lentiginoses: cutaneous markers of systemic disease and a window to new aspects of tumourigenesis. *J. Med. Genet.*, **42**, 801–810.
32. Budovskaya, Y.V., Stephan, J.S., Deminoff, S.J. and Herman, P.K. (2005) An evolutionary proteomics approach identifies substrates of the cAMP-dependent protein kinase. *Proc. Natl Acad. Sci. USA*, **102**, 13933–13938.
33. Giaever, G., Chu, A.M., Ni, L., Connelly, C., Riles, L., Veronneau, S., Dow, S., Lucau-Danila, A., Anderson, K., Andre, B. *et al*. (2002) Functional profiling of the *Saccharomyces cerevisiae* genome. *Nature*, **418**, 387–391.
34. Schmelzle, T., Beck, T., Martin, D.E. and Hall, M.N. (2004) Activation of the RAS/cyclic AMP pathway suppresses a TOR deficiency in yeast. *Mol. Cell Biol.*, **24**, 338–351.
35. Bonner, R.F., Emmert-Buck, M., Cole, K., Pohida, T., Chuaqui, R., Goldstein, S. and Liotta, L.A. (1997) Laser capture microdissection: molecular analysis of tissue. *Science*, **278**, 1481–1483.
36. Nadella, K.S. and Kirschner, L.S. (2005) Disruption of protein kinase a regulation causes immortalization and dysregulation of D-type cyclins. *Cancer Res.*, **65**, 10307–10315.
37. Lorenz, H., Hailey, D.W. and Lippincott-Schwartz, J. (2006) Fluorescence protease protection of GFP chimeras to reveal protein topology and subcellular localization. *Nat. Methods*, **3**, 205–210.
38. Ward, T.H., Polishchuk, R.S., Caplan, S., Hirschberg, K. and Lippincott-Schwartz, J. (2001) Maintenance of Golgi structure and function depends on the integrity of ER export. *J. Cell Biol.*, **155**, 557–570.
39. Groussin, L., Kirschner, L.S., Vincent-Dejean, C., Perlemoine, K., Jullian, E., Delemer, B., Zacharieva, S., Pignatelli, D., Carney, J.A., Luton, J.P. *et al*. (2002) Molecular analysis of the cyclic AMP-dependent protein kinase A (PKA) regulatory subunit 1A (PRKAR1A) gene in patients with Carney complex and primary pigmented nodular adrenocortical disease (PPNAD) reveals novel mutations and clues for pathophysiology: augmented PKA signaling is associated with adrenal tumorigenesis in PPNAD. *Am. J. Hum. Genet.*, **71**, 1433–1442.
40. Stratakis, C.A., Carney, J.A., Kirschner, L.S., Willenberg, H.S., Brauer, S., Ehrhart-Bornstein, M. and Bornstein, S.R. (1999) Synaptophysin immunoreactivity in primary pigmented nodular adrenocortical disease: neuroendocrine properties of tumors associated with Carney complex. *J. Clin. Endocrinol. Metab.*, **84**, 1122–1128.
41. Snapp, E.L., Altan, N. and Lippincott-Schwartz, J. (2003) Measuring protein mobility by photobleaching GFP-chimeras in living cells. Bonifacino, J., Dasso, M., Harford, J., Lippincott-Schwartz, J. and Yamada, K. (Eds), *Current protocols in Cell Biology*, John Wiley & Sons, New York.